Analytical model for Rayleigh–Brillouin line shapes in air

B. Witschas

Deutsches Zentrum für Luft- und Raumfahrt, Institut für Physik der Atmosphäre, Oberpfaffenhofen, Germany

Friedrich Schiller Universität Jena, Institut für Angewandte Physik, Albert-Einstein-Strasse 15, 07745 Jena, Germany (Benjamin.Witschas@dlr.de)

Received 21 September 2010; revised 12 November 2010; accepted 26 November 2010; posted 3 December 2010 (Doc. ID 135280); published 13 January 2011

Atmospheric lidar techniques for the measurement of wind, temperature, and optical properties of aerosols as well as nonintrusive measurement techniques for temperature, density, and bulk velocity in gas flows rely on the exact knowledge of the spectral line shape of the scattered laser light on molecules. A mathematically complex, numerical model (Tenti S6 model) is currently the best model for describing these spectra. In this paper an easy processable, alternative analytical model for describing spontaneous Rayleigh–Brillouin spectra in air at atmospheric conditions is introduced. The deviations between the analytical and Tenti S6 models are shown to be smaller than 0.85%.

OCIS codes: 280.3640, 280.1310, 120.1740, 280.2490.

The quasi-elastic scattering of laser light by molecular gases, known as spontaneous Rayleigh–Brillouin (SRB) scattering, is widely used in atmospheric remote sensing applications such as lidar (light detection and ranging) [1–3], as well as in nonintrusive diagnostic tools in aerospace applications such as combustion [4] and flow measurements [5]. Whereas the spectrum of the scattered light is needed to retrieve the aerosol content from high spectral resolution lidar data [2] and the wind speed from direct detection wind lidar data [6], it is used to derive the temperature, density, and bulk velocity of the scattering gas medium by comparing the measured SRB spectrum with appropriate line shape models in combustion and flow measurements [4,5].

Basically, the spectrum of SRB scattered light is an image of the velocity distribution of the molecules in the scattering medium, and therefore, it contains information on gas transport properties like heat capacity, thermal conductivity, shear and bulk viscosity as well as on temperature, density (pressure), and bulk velocity. The spectrum of SRB scattered light is commonly expressed as a function of two nondimensional parameters [7],

$$x = \frac{\omega}{\sqrt{2}kv_0}, \qquad y = \frac{nk_BT}{\sqrt{2}kv_0\eta} = \frac{p}{\sqrt{2}kv_0\eta}, \tag{1}$$

where ω is the angular frequency shift between scattered and incident light, n is the number density, p and T are the gas pressure and temperature, η is the shear viscosity, $k = \boldsymbol{k_s} - \boldsymbol{k_0} = 4\pi/\lambda \sin(\theta/2)$ is the magnitude of the interacting wave vector (with $\boldsymbol{k_0}$ and $\boldsymbol{k_s}$ being the wave vectors of the incident and scattered light), λ is the wavelength of the incident light, θ is the scattering angle, and $v_0 = (k_BT/m)^{(1/2)}$ the thermal velocity (with k_B being the Boltzmann constant and m the molecular mass). Thus, x is the optical frequency shift and y the collision frequency, both normalized with respect to $\sqrt{2}kv_0$, which is of the order of the frequency of sound waves in the gas. This gives the possibility to view y as the ratio of the acoustic wavelength to the mean free path between collisions.

For discussing the origin of SRB line shapes, it is useful to define different scattering regimes for different y values. In the Knudsen regime ($y \ll 1$),

0003-6935/11/030267-04$15.00/0

the mean free path between collisions is much larger than the acoustic wavelength and the line profile of the scattered light is described by a Gaussian function [6]. In the hydrodynamic regime ($y \gg 1$), the mean free path between collisions is much smaller than the acoustic wavelength and the spectrum of the scattered light is composed of three Lorentzian functions: a central Rayleigh peak and two displaced Brillouin peaks [8]. In the kinetic regime ($0.1 \lesssim y \lesssim 3$), which is the relevant regime for most atmospheric applications (e.g., $y = 0.05 - 0.4$ for lidar measurements with ultraviolet laser light [6]), the mean free path between collisions is of the order of the acoustic wavelength. To describe the spectrum of the scattered light in that case, one has to resort to solutions of the Boltzmann equation for the density fluctuations [9,10] to get information about the velocity distribution of the molecules, and therefore, about the SRB spectrum. Thus, there is no analytical solution possible for this equation, only approximative models can be derived.

Based on an approximate solution of the linearized Boltzmann equation, Boley *et al.* and Tenti *et al.* [7,11] described a model (Tenti S6 model) for the spectral line shape of scattered radiation that has widely been applied in atmospheric and aerospace applications [1–6]. Although the Tenti S6 model was developed for gases of a single-component molecular species and not for gas mixtures such as air, it was recently shown that it is also adequate for the latter case [9,10].

However, the mathematically complex, nonanalytical closed form of the Tenti S6 model makes the application to measured data quite circuitous. For example, deriving the temperature from the measured SRB line shape can only be performed by complicated numerical fit procedures, instead of using ordinary least square fit routines as it is common for analytical functions. For the wind retrieval in the frame of the ADM-Aeolus mission, extensive look-up tables for SRB line shapes at different y values has to be calculated. In addition, further processing of the Tenti S6 modeled spectra, e.g. convolution with the instrument function of the measurement system, is hard to achieve. To overcome this situation, an easy processable analytical representation of the Tenti S6 model is empirically derived for SRB spectra in air.

The basic concept of the analytical model is to describe the SRB spectrum $\mathcal{S}(x,y)$ in the style of the hydrodynamic regime by superposing a central Gaussian line with standard deviation σ_R and integrated intensity $\mathcal{A}$ to represent the Rayleigh peak, and two shifted Gaussian lines at $\pm x_B$ with standard deviation σ_B and integrated intensity $(1-\mathcal{A})/2$ to represent the Brillouin doublet (see Fig. 1).

With $0 \le \mathcal{A} \le 1$, the analytically calculated spectrum $\mathcal{S}(x,y)$ is normalized to unity integrated intensity and can be written as

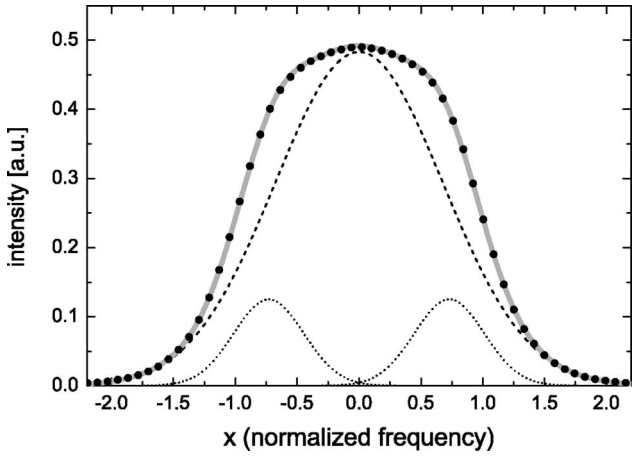

Fig. 1. Spectrum of SRB scattered light in air for $y = 0.652$ according to the Tenti S6 model (black dots). The gray line represents the superposition of a central Gaussian line with standard deviation $\sigma_R = 0.68$ and integrated intensity $\mathcal{A} = 0.82$ (dashed black line) and two shifted Gaussian lines at $\pm x_B = 0.73$ with standard deviation $\sigma_B = 0.28$, and integrated intensity $(1-\mathcal{A})/2 = 0.09$ (dotted black line). The Tenti modeled line shape as well as the superposition of the Gaussians is normalized to yield unity integrated intensity.

$$\mathcal{S}(x,y) = \frac{1}{\sqrt{2\pi}\sigma_R}\mathcal{A}\exp\left[-\frac{1}{2}\left(\frac{x}{\sigma_R}\right)^2\right] + \frac{1-\mathcal{A}}{2\sqrt{2\pi}\,\sigma_B}\exp\left[-\frac{1}{2}\left(\frac{x+x_B}{\sigma_B}\right)^2\right] + \frac{1-\mathcal{A}}{2\sqrt{2\pi}\,\sigma_B}\exp\left[-\frac{1}{2}\left(\frac{x-x_B}{\sigma_B}\right)^2\right]. \quad (2)$$

In contrast to similar approaches as introduced by Gustavsson [12] and Zheng [13], the parameters $\mathcal{A}$, σ_R, σ_B, and x_B are now determined solely empirically to obtain the best accordance between $\mathcal{S}(x,y)$ and the Tenti S6 model.

Actually, the S6 spectrum is depending on four dimensionless parameters which are x and y from Eq. (1), $z = \eta/\eta_B$ and $f = (m\kappa)/(k_B\eta)$, where η_B is the bulk viscosity and κ the thermal conductivity of the scattering medium. However, for atmospheric applications, z and f can be approximated to be constant with respect to temperature [14,15], although there is a strong demand to prove this approximation with measurements. Taking the transport coefficients of air ($m = 4.789 \cdot 10^{-26}$ kg, $\eta = 1.846 \cdot 10^{-5}$ Pa m^{-1} s^{-1}, $\eta_B = 1.5 \cdot 10^{-5}$ Pa m^{-1} s^{-1}, $\kappa = 2.624 \cdot 10^{-2}$ W m^{-1} K^{-1}, $\gamma = 1.4$) [9,15], $z = 1.231$ and $f = 4.934$. Now, a set of Tenti spectra is calculated for atmospheric conditions representing y values between 0 and 1.027. After that, these spectra are fitted with Eq. (2) in a least square fit procedure to find best fit values for $\mathcal{A}$, σ_R, σ_B, and x_B. For the case of $y = 0$, $\mathcal{A}$ is restricted to be unity, and therefore, $\mathcal{S}(x,y)$ is only composed of the central Gaussian line with a standard deviation σ_R of the Maxwellian velocity distribution. This approach results in a set of $\mathcal{A}$, σ_R, σ_B, and x_B values, depending on y (Fig. 2,

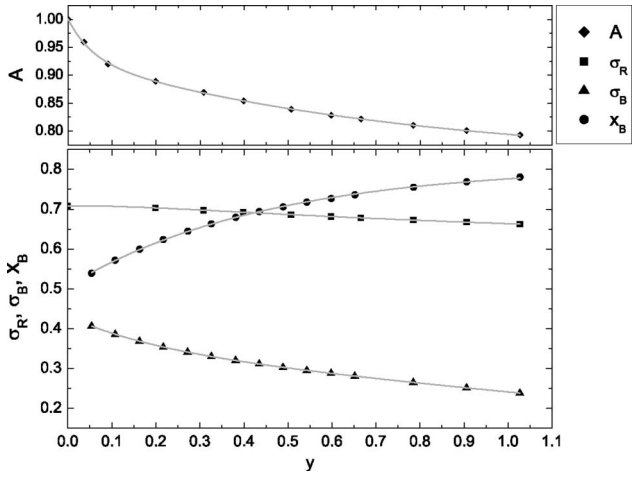

Fig. 2. Integrated intensity $\mathcal{A}$ of the central peak (top, black diamonds), the standard deviation σ_R of the central peak (bottom, black squares), the standard deviation σ_B of the side peaks (bottom, black triangles) and the frequency shift x_B of the side peaks (bottom, black circles), determined by applying Eq. (2) to a set of Tenti S6 modeled line shapes ($y = 0 - 1.027$) in a least square fit procedure. The gray lines depict well fitting functions which are given by Eqs. (3)–(6), respectively.

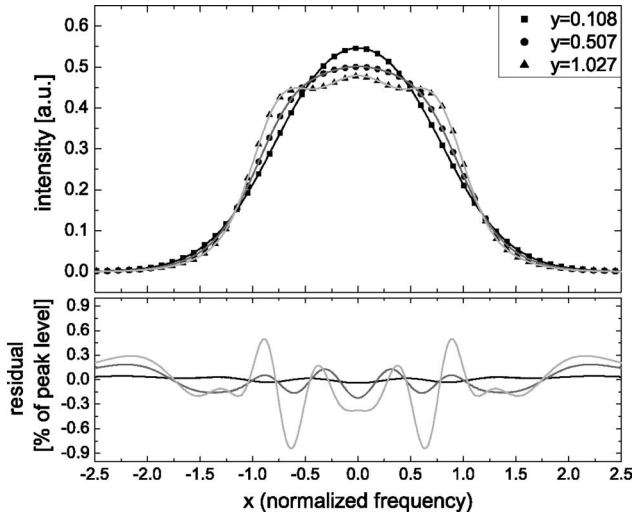

Fig. 3. (Top) Tenti modeled line shapes for $y = 0.108$ (black square), $y = 0.507$ (black circles), $y = 1.027$ (black triangles), and the best fit of Eq. (2) in black, dark gray, and light gray, respectively. (Bottom) Residual between Tenti model and analytical model with respect to peak intensity.

symbols). Now, these values are fitted with appropriate mathematical functions which result in

$$\mathcal{A}(y) = 0.18526 \cdot \exp[-1.31255y] + 0.07103 \cdot \exp[-18.26117y] + 0.74421, \quad (3)$$

$$\sigma_R(y) = 0.70813 + 0.16366y^2 + 0.19132y^3 - 0.07217y^4, \quad (4)$$

$$\sigma_B(y) = 0.07845 \cdot \exp[-4.88663y] + 0.80400 \cdot \exp[-0.15003y] - 0.45142, \quad (5)$$

$$x_B(y) = 0.80893 - 0.30208 \cdot 0.10898^y \quad (6)$$

The obtained best fit values for $\mathcal{A}$, σ_R, σ_B, and x_B as well as the describing model functions [Eqs. (3)–(6)] are sketched in Fig. 2.

Applying Eqs. (3)–(6) to Eq. (2), an analytical formula for describing SRB line shapes in air valid for $y = 0 - 1.027$ is introduced. It is worth mentioning that this method can also be performed for other gases, and therefore, gives the possibility to derive an analytical model for SRB line shapes for respective applications.

The goal of the presented approach was the development of an easy processable analytical representation of the Tenti S6 model for SRB line shapes in air for the kinetic regime ($y = 0 - 1.027$). To demonstrate that this goal is met by the derived model, a direct comparison to the Tenti S6 model is performed by fitting Eqs. (2)–(6) to a set of Tenti S6 lines. The accuracy of representation is thereby quantified by calculating the residual between the Tenti S6 spectrum $\mathcal{S}_T(x,y)$ and the analytically modeled spectrum $\mathcal{S}_A(x,y)$ with respect to the peak intensity $\mathcal{S}_T(0,y)$ according to $((\mathcal{S}_T(x,y) - \mathcal{S}_A(x,y))/\mathcal{S}_T(0,y))$. Examples for $y = 0.108$, $y = 0.507$, and $y = 1.027$ are plotted in Fig. 3.

Figure 3 makes obvious that the deviations between both models are smaller than 0.18% for $y \leq 0.5$ and therefore the analytical model is an almost perfect image of the Tenti S6 model in that region. The deviations between both models start to increase for increasing y values (e.g., 0.85% for $y = 1.027$), which demonstrates that the accordance between the analytical model and the Tenti S6 model is directly depending on y, and that the presented model is restricted to the region $y \leq 1$. However, that is the most relevant region for atmospheric remote sensing and aerospace applications [2–6].

In conclusion, an easy processable analytical model for the description of SRB line shapes in air was derived. The model is valid for $y = 0 - 1.027$ and the deviations to the Tenti S6 model are smaller than 0.85% within that region. Therefore, the model was derived using the dimensionless parameters x and y; it can be applied to various applications with different setup configurations.

The review and valuable comments by Oliver Reitebuch and Christian Lemmerz are highly appreciated. Thomas Trickl provided very helpful suggestions and comments as well as his first experience with the presented line shape model. The comments of an anonymous reviewer are gratefully acknowledged.

References

1. O. Reitebuch, C. Lemmerz, E. Nagel, and U. Paffrath, "The airborne demonstrator for the direct-detection Doppler wind lidar ALADIN on ADM-aeolus. Part I: Instrument design

and comparison to satellite instrument," J. Atmos. Ocean. Technol. **26**, 2501–2515 (2009).
2. B. Y. Liu, M. Esselborn, M. Wirth, A. Fix, D. B. Bi, and G. Ehret, "Influence of molecular scattering models on aerosol optical properties measured by high spectral resolution lidar," Appl. Opt. **48**, 5143–5153 (2009).
3. Z.-S. Liu, D.-C. Bi, X.-Q. Song, J.-B. Xia, R.-Z. Li, Z.-J. Wang, and C.-Y. She, "Iodine-filter-based high spectral resolution lidar for atmospheric temperature measurements," Opt. Lett. **34**, 2712–2714 (2009).
4. G. Elliott, N. Glumac, and C. Carter, "Molecular filtered Rayleigh scattering applied to combustion," Meas. Sci. Technol. **12**, 452–466 (2001).
5. R. Seasholtz, A. Buggele, and M. Reeder, "Flow measurements based on Rayleigh scattering and Fabry-Perot interferometer," Opt. Lasers Eng. **27**, 543–570 (1997).
6. A. Dabas, M. Denneulin, P. Flamant, C. Loth, A. Garnier, and A. Dolfi-Bouteyre, "Correcting winds measured with a Rayleigh Doppler lidar from pressure and temperature effects," Tellus A **60**, 206–215 (2008).
7. G. Tenti, C. Boley, and R. Desai, "On the kinetic model description of Rayleigh-Brillouin scattering from molecular gases," Can. J. Phys. **52**, 285–290 (1974).
8. J. P. Boon and S. Yip, *Molecular Hydrodynamics* (McGraw-Hill, 1980), pp. 246–254.
9. B. Witschas, M. O. Vieitez, E.-J. van Duijn, O. Reitebuch, W. van de Water, and W. Ubachs, "Spontaneous Rayleigh–Brillouin scattering of ultraviolet light in nitrogen, dry air, and moist air," Appl. Opt. **49**, 4217–4227 (2010).
10. M. O. Vieitez, E. J. van Duijn, W. Ubachs, B. Witschas, A. Meijer, A. S. de Wijn, N. J. Dam, and W. van de Water, "Coherent and spontaneous Rayleigh-Brillouin scattering in atomic and molecular gases and gas mixtures," Phys. Rev. A **82**, 0438361–14 (2010).
11. C. D. Boley, R. C. Desai, and G. Tenti, "Kinetic models and Brillouin scattering in a molecular gas," Can. J. Phys. **50**, 2158 (1972).
12. J. Gustavsson, "Molecular velocity distribution in air," http://plaza.ufl.edu/jgu/public_html/UF/AirMolVelDistr.pdf.
13. Q. Zheng, "On the Rayleigh-Brillouin scattering in air," Ph.D. dissertation (University of New Hampshire, 2004).
14. H. Shimizu, K. Noguchi, and C. Y. She, "Atmospheric temperature measurement by a high spectral resolution lidar," Appl. Opt. **25**, 1460–1466 (1986).
15. T. D. Rossing, ed., *Springer Handbook of Acoustics* (Springer, 2007), p. 31.